On the modelling of a lime carbonator operating in a concentrated solar power plant for energy storage

Manuel Bailera[a], Pilar Lisbona[a], Sara Pascual[a], Luis I. Díez[a] and Luis M. Romeo[a]

[a]Energía y CO_2. Department of Mechanical Engineering. Escuela de Ingeniería y Arquitectura. Universidad de Zaragoza, Campus Río Ebro, María de Luna 3, 50018, Zaragoza, Spain

Abstract:

Calcium-looping systems can be integrated in concentrated solar power plants serving as an energy storage alternative. This concept is based in the reversible calcination-carbonation reaction, in which limestone and lime are alternatively converted, generating and using CO_2 and introducing (storing) or releasing important quantities of energy. Energy from concentrated solar power (CSP) can be stored by limestone calcination (endothermic reaction) at high temperatures producing pure streams of CaO and CO_2. This energy can be used when demand increases by means of carbonation reaction (exothermic) at relatively high temperatures suitable for Rankine cycles. Carbonator reactor is a complex system where heterogeneous chemical reactions take place together with heat release and heat transfer to the production of steam for the Rankine cycle. It is a key element of the process. In this work the modelling of a future commercial-scale carbonator is described, in the frame of a new solar-based plant. The reactor has been considered with a downward entrained flow design, and the model encompasses fluid dynamics, chemical kinetics and energy balance. The results, provided along a 1-D discretization, comprise conversion rates, gas temperatures and flow rates, and heat transfer rates to the external cooling fluid. The round trip efficiency of the energy storage technology is assessed for different carbonator dimensions.

Keywords:

Calcium-looping, Energy storage, Concentrated solar power, CO2, Carbonation.

1. Introduction

One of the near-term energy challenges is the necessity to develop and deploy efficient and non-expensive technologies for energy storage. The renewable energy production must grow in parallel with energy storage systems that overcome their intrinsic variability. There are several possibilities for storing energy that depends on the renewable energy source, the time displacement of the energy, the storage period, prices and materials.

In particular, concentrated solar power needs energy storage to overcome the daily load variability and night periods. Besides, thermal energy storage systems operating at medium to high temperature level are preferred in CSP in order to achieve a high round-trip efficiency. Usually, molten salt systems [1] are used in commercial installations. Nevertheless, other possibilities as mineral oils or ceramic materials are under research [2]. In the last years thermochemical energy

storage (TCES) has been proposed as an innovative possibility to solve the variability of CSP production. In this option, energy is storage in the form of thermal energy combined with an endothermic chemical reaction. One of the main advantages is that the density of the storage is larger than in other alternatives. To take advantage of the stored energy, the reverse exothermic reaction is used.

Several possibilities for TCES have been proposed [3]. The use of $CaCO_3$ is an interesting alternative due to the large experience in the carbonation/calcination reaction, its abundancy and its low price. The Ca-Looping (CaL) process has been lately used as an option for CO_2 capture [4][5][6] but it has been also proposed for being used in CSP plants [7][8]. The Ca-Looping (CaL) process is based upon the reversible carbonation/calcination of CaO in which limestone and lime are alternatively converted, generating and using CO_2 and introducing (storing) or releasing important quantities of energy. Energy from CSP can be stored by limestone calcination (endothermic reaction) at high temperatures producing pure streams of CaO and CO_2. This energy can be used when demand increases by means of carbonation reaction (exothermic) at relatively high temperatures. In order to produce power, this energy has to be transferred to a Rankine cycle [8] or other types of power cycles [7]. Previous works have demonstrated an outstanding performance in both situations, for a regenerative Rankine cycle an efficiency of 35.5% has been presented, but it increases to near 39.0% for a combined cycle or 42.0% for a closed Brayton cycle [8].

To achieve this favourable efficiency figures, proper designs of the main reactors (carbonator and calciner) have to be proposed. The design has to deal with process and reactor limitations that can weaken the performance of the overall system. The main restriction is the reduction of particle size in comparison with well-known Ca-L processes for carbon capture. Particle size of tens of microns allows an adequate calcination using solar energy but it has important implication in the design of both, calciner and carbonator.

Carbonator reactor is a complex system where heterogeneous chemical reactions take place together with heat release and heat transfer to the production of steam for the Rankine cycle. It is a key element of the process. Several works in literature have been proposed and have shown the simulation results of carbonator for carbon capture applications [9][10]. No attempt has been made for the design of the carbonator for a CSP installation. This is the objective of this paper. In this work the modelling of a future commercial-scale carbonator is described, in the frame of a new solar-based plant. Different lengths and diameters for a commercial carbonator are analysed, as well as the corresponding heat released.

2. Calcium-looping as energy storage technology: Carbonator

The carbonator is a co-current entrained flow reactor covered with four helical coiled heat exchangers in which pressurized water enters at 300 bar and 350 ºC (Fig. 1). The CaO and CO_2 inlet mass flow rates are 73.41 kg/s and 57.62 kg/s, respectively, which correspond to solar thermal powers of 100 MWth inside the calciner.

Assuming a 13.3% conversion inside the carbonator (maximum residual conversion for sintered material), the outlet mass flows will be 17.31 kg/s of $CaCO_3$, 63.71 kg/s of CaO, and 50.00 kg/s of CO_2. The gas is separated from the solids and recirculated to the carbonator's inlet, thus avoiding preheating (i.e., 86.7% of the inlet CO_2 is actually in closed loop). The solids are cooled down and stored to be later used again in the calciner, where the 100 MWth (inlet solar power) are distributed between heating the material from room temperature and calcining the 100% of the $CaCO_3$ that is present in the mixture.

The outlet conditions of the cooling fluid are set in order to achieve 600 ºC and a maximum pressure loss of 20 bar. Thus, the simulation will provide as results the required mass flows and the diameters of the helical coiled tubes.

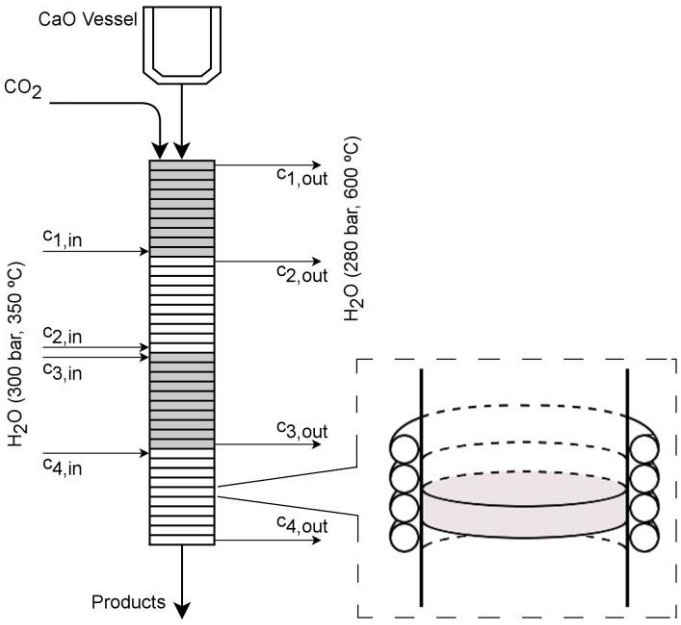

Figure 1. Conceptual design of the carbonator.

3. Methodology

This model takes geometry, heat transfer and calcination kinetics into account, thus obtaining the temperature profiles along the carbonator under non-isothermal conditions. The model is in steady-state and has been implemented in EES (Engineering Equation Solver). To calculate the residence time of the gas in the carbonator, 1D plug flow is considered. The entraining velocity in downflow for the solid is calculated through the terminal velocity and the gas velocity. The reactor has been discretized in slides of 2 cm length.

3.1. Carbonation kinetic model

The kinetic model is the one published by Ortiz et al [11], in which different fitting parameters have been used, coming from the experimental tests of the SOCRATCES project. Thus, the carbonation reaction is described by (1), which gives the conversion of CaO as a function of time:

$$X(t) = \frac{X_k}{1 + e^{-r(t-t_0)}} \tag{1}$$

where X_k is the conversion at the end of the reaction controlled phase and t_0 the time taken to reach a $X_k/2$ conversion. In addition, the reaction rate r is given by (2) as a function of temperature and CO_2 partial pressure:

$$r = a_2 \cdot e^{\left(-\frac{E_2}{\mathcal{R}T}\right)} \cdot \left(\frac{P}{P_{eq}} - 1\right) \cdot \left(\frac{1}{\frac{P}{P_{eq}} + e^{\left(\Delta S_2^0/\mathcal{R}\right)} e^{\left(-\Delta H_2^0/\mathcal{R}T_s\right)}}\right) \tag{2}$$

where E_2 is 20 kJ/mol, ΔS_2^0 is -68 J/mol·K and ΔH_2^0 is -160 kJ/mol. Besides, $P_{eq} = \mathcal{A} \cdot \exp(-a/T)$, where $\mathcal{A}$ is $4.083 \cdot 10^7$ atm, and a is 20474 K.

The kinetic model allows computing the mole flow of each component as a function of time. Therefore, in order to characterize the carbonator based on its dimensions, it is required to know how long the solid and the gas are interacting as they flow down through the reactor.

3.2. Residence time for the solids

The time of interaction between the solid and the gas is limited to the residence time of the solid in the carbonator. For those flows with Reynolds lower than 2 and small size particles, the following (3) may be applied for the downward velocity of single particles, v_s, (concentration of particles is assumed diluted) [12]:

$$v_s = v_{s,i} \cdot e^{-bt_s} + \left(v_g + v_t\right) \cdot (1 - e^{-bt_s}) \tag{3}$$

where $v_{s,i}$ is the initial velocity of the solid, v_g is the velocity of the gas phase, and v_t is the terminal settling velocity of the particle in a static fluid. The parameter b, and the velocity v_t are given by (4) and (5):

$$b = \frac{18\mu}{\rho_s d_p^2} \tag{4}$$

$$v_t = \frac{\left(\rho_s + \rho_g\right) d_p^2 g}{18\mu} \tag{5}$$

where μ is the viscosity of the gas, ρ_s is the density of the solid, ρ_g is the density of the gas, d_p is the diameter of the solid particles, and g the gravity.

The integration of (3) provides the relationship between the carbonator length and the residence time of the solids (6).

$$L = \int_0^{t_{s,L}} v_s dt_s = \frac{v_{s,i}}{b}(1 - e^{-bt_s}) + \left(v_g + v_t\right) \cdot \left(t_s - \frac{1 - e^{-bt_s}}{b}\right) \tag{6}$$

It can be assumed that v_g and μ are constants in the interval of integration for the case of study. Thus, this can be directly solved by the EES software to compute the residence time of the solid as a function of the length, what will allow determining the mole flows along the reactor as a function of the distance from the entrance.

3.3. Plug flow model (1D) for the gas phase

The residence time of the gas is given by (7):

$$t_g = \int_0^{V_c} \frac{\pi r_{in}^2}{\dot{V}} dL \tag{7}$$

where r_{in} is the inner radius of the carbonator, $\dot{V}$ is the volumetric flow rate, and V_c the carbonator volume. Moreover, $\dot{V}$ is the product of the gas velocity multiplied by the cross-sectional area of the reactor, which must be corrected by subtracting the area occupied by the solids. The variation in the effective cross-sectional area along the reactor may be neglected as $CaCO_3$ is produced when CaO is consumed.

Besides, it is assumed that the pressure inside the reactor remains constant at 1.7 bar. Hence, the volumetric flow rate is given by (8), according to the ideal gas law:

$$\dot{V}_{L2} = \frac{(1 - X_{L2}) \cdot T_{L2}}{T_{L1}} \dot{V}_{L1} \tag{8}$$

The residence time of the gas, through a length L_i in which $\dot{V}_{Li}$ can be considered constant will be $t_{g(L1)} = L_i \cdot S_{eff}/\dot{V}_{Li}$.

3.4. Heat transfer model

The carbonator is covered with helical coiled heat exchangers acting as cooling jacket. The following steps are taken to compute the heat transfer from the cloud of gas and particles to the cooling fluid. First, an energy balance inside the reactor is computed for each slice of reactor (from length L_{i-1} to length L_i) by (9):

$$\sum_j Cp_j \cdot \dot{n}_{j,L_i} \cdot \left(T_{L_i} - T_{L_{i-1}}\right) = -\Delta H_r \cdot \left(\dot{n}_{CaCO3,L_i} - \dot{n}_{CaCO3,L_{i-1}}\right) - \dot{q}'_{L_i} \cdot (L_i - L_{i-1}) \tag{9}$$

where Cp_j and $\dot{n}_{j,}$ are the specific heat and mole flow of component j, respectively, T is the temperature of the cloud of gas and particles (which is assumed homogeneous inside the carbonator), ΔH_r is the enthalpy of reaction (-178 kJ/mol), and $\dot{q}'_{L_i}$ is the heat flow throughout the inside wall of the carbonator per unit of length. The latter accounts for radiation and convection, in the form of (10):

$$\dot{q}'_{L_i} = \dot{q}'_{rad,L_i} + \dot{q}'_{conv,L_i} \tag{10}$$

$$\dot{q}'_{rad,L_i} = \frac{\varepsilon_w}{\alpha_{g+p} + \varepsilon_w - \alpha_{g+p} \cdot \varepsilon_w} \cdot \sigma \cdot (\varepsilon_{g+p} \cdot T_{L_i}^4 - \alpha_{g+p} \cdot T_{iw,L_i}^4) \cdot 2\pi r \tag{11}$$

$$\dot{q}'_{conv,L_i} = h_{g,L_i} \cdot \left(T_{L_i} - T_{iw,L_i}\right) \cdot 2\pi r \tag{12}$$

Where α_{g+p} and ε_{g+p} are the absorptivity and emissivity of the gas-particle mixture, ε_w the emissivity of the carbonator wall, σ is the Stefan-Boltzmann constant, T_{iw} is the temperature of the inner wall of the carbonator, r the inner radius of the carbonator, and h_g the convective coefficient.

The model for the calculation of the absorptivity and emissivity of the gas-particle mixture is borne out of the VDI Heat Atlas, Part K [13]. The total emissivity of a gas-particle mixture can be described as

$$\varepsilon_{g+p} = (1 - \beta)\left(\frac{1 - \exp\left(-\Phi_{emi,g+p}\right)}{1 + \beta \exp\left(-\Phi_{emi,g+p}\right)}\right) \tag{13}$$

Where

$$\gamma = \sqrt{1 + \frac{2\bar{Q}_{bsc}}{\bar{Q}_{abs}}} \tag{14}$$

$$\beta = \frac{\gamma - 1}{\gamma + 1} \tag{15}$$

$$\Phi_{emi,g+p} = \left(\bar{Q}_{abs} A L_p + K_{emi,g}\right) l_{mb} \gamma \tag{16}$$

In a similar manner the absorptivity can be calculated:

$$\alpha_{g+p} = (1 - \beta)\left(\frac{1 - \exp\left(-\Phi_{abs,g+p}\right)}{1 + \beta \exp\left(-\Phi_{abs,g+p}\right)}\right) \tag{17}$$

Where

$$\Phi_{abs,g+p} = \left(\bar{Q}_{abs} A L_p + K_{abs,g}\right) l_{mb} \gamma \tag{18}$$

L_p is the particle loading, in kg/m^3. The parameter l_{mb} is the mean beam length of radiation within the relevant geometry. A is the specific surface area of the particles.

The determination of particle absorption and scattering coefficients $\bar{Q}_{abs}$ and $\bar{Q}_{bsc}$ is performed graphically, and limestone is included on the graph in the Heat Atlas. The mean particle diameter d_p is measured experimentally, or can be calculated from the surface area and density of the particles by

$$d_p = \frac{3}{2\rho_p A} \tag{19}$$

The gas absorption and scattering coefficients are defined as

$$K_{emi,g} = -\frac{\ln\left(1 - \varepsilon_g\right)}{l_{mb}} \tag{20}$$

$$K_{abs,g} = -\frac{\ln(1 - A_v)}{l_{mb}} \tag{21}$$

Where ε_g is the emissivity of the gas and A_v is the absorptance. The value of ε_g varies with pressure, optical thickness and temperature. It is found using a graph in the Heat Atlas [13]. The absorptance A_v is a function of the wall and gas temperatures and the emissivity of the gas:

$$A_v = f_{p,CO_2}\left(\frac{T_g}{T_w}\right)^{0.65} \varepsilon_g \tag{22}$$

The parameter f_{p,CO_2} is a pressure correction factor that at 1.0 bar total pressure is equal to 1.000, and at 1.7 bar is equal to 1.018.

Besides, the model for the calculation of the convective coefficient is borne out of ‘Heat Transfer’ by Nellis G and Klein S [14], and follows (23) to (27):

$$h_{g,L_i} = \frac{Nu_{Li} \cdot k_{Li}}{2r} \tag{23}$$

$$Nu_{L_i} = 3.66 + \frac{\left(0.049 + \frac{0.020}{Pr_{Li}}\right) \cdot Gz_{Li}^{1.12}}{1 + 0.065 \cdot Gz_{Li}^{0.7}} \tag{24}$$

$$Pr_{Li} = \frac{Cp_{Li} \cdot \mu_{Li}}{k_{Li}} \tag{25}$$

$$Gz_{Li} = \frac{Re_{Li} \cdot Pr_{Li}}{L/2r} \tag{26}$$

$$Re_{Li} = \frac{4 \cdot \dot{m}_{Li}}{\pi \cdot 2r \cdot \mu_{Li}} \tag{27}$$

where Nu is the Nusselt number, k the thermal conductivity, Pr the Prandtl number, Gz the Graetz number, μ the viscosity, Re the Reynolds number, and $\dot{m}$ the mass flow.

The temperature of the outer wall of the carbonator, T_{ow}, is computed by the formula of heat conduction through a tube wall (28):

$$\dot{q}'_{L_i} = \frac{T_{iw,L_i} - T_{ow,L_i}}{R_{tube} \cdot L_i} \tag{28}$$

$$R_{tube} = \frac{\ln(\frac{r_{out}}{r})}{2\pi \cdot k_{tube} \cdot L_i} \tag{29}$$

where R_{tube} is the thermal resistance of the carbonator tube, r_{out} the outer radius of the carbonator, and k_{tube} the thermal conductivity of the carbonator tube (0.025 kW/m·K).

Then, it is assumed that the temperature of the carbonator's outer wall is equal to the temperature of the cooling fluid inside the helical pipe, since the convective coefficient inside the helical pipe is several orders of magnitude greater than inside the carbonator. Thus, the following energy balance on the cooling fluid is computed (30):

$$Cp_{cf} \cdot \dot{n}_{cf} \cdot \left(T_{ow,L_i-1} - T_{ow,L_i}\right) = \dot{q}'_{L_i} \cdot (L_i - L_{i-1}) \tag{30}$$

Where Cp_{cf} and $\dot{n}_{cf}$ are the specific heat and the mole flow of the cooling fluid. It should be noted that (30) is valid for those heat exchangers in which the cooling fluid flows from bottom to top (counter-current), and therefore it is heated from position L_i to L_{i-1}, with the heat produced inside the carbonator from position L_{i-1} to L_i. In case of evaluating a co-current heat exchanger, the energy balance is given by (31), where the cooling fluid flows from top to bottom.

$$Cp_{cf} \cdot \dot{n}_{cf} \cdot \left(T_{ow,L_i} - T_{ow,L_i-1}\right) = \dot{q}'_{L_i} \cdot (L_i - L_{i-1}) \tag{31}$$

Thus, the temperature along the carbonator can be computed by knowing the initial temperature of the cooling fluid.

4. Results

Due to the scale of the studied system (100 MWth net solar input), the length required in the carbonator to achieve conversions above 12% varies between 37 m and 56 m, for diameters between 7 m and 4 m, respectively (Fig. 2). To increase conversion from 12% to about 13.2% (i.e., close to the maximum), increments of length of 15 – 17 m are required. Thus, for 7 m diameters, a length of 52 m would be needed.

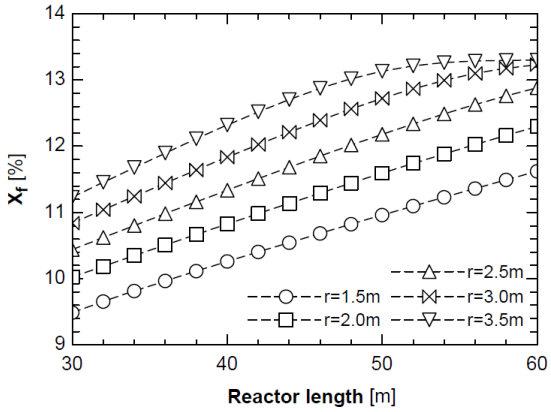

Figure 2. Final conversion vs. reactor's length and radius dimensions.

The exothermal power produced in the carbonation reaction is about 28.4 MW for 12% conversions. In the case of the 7 m in diameter and 52 in length carbonator with 13.2% final conversion, the thermal power released during carbonation is 31.1 MW (Fig. 3).

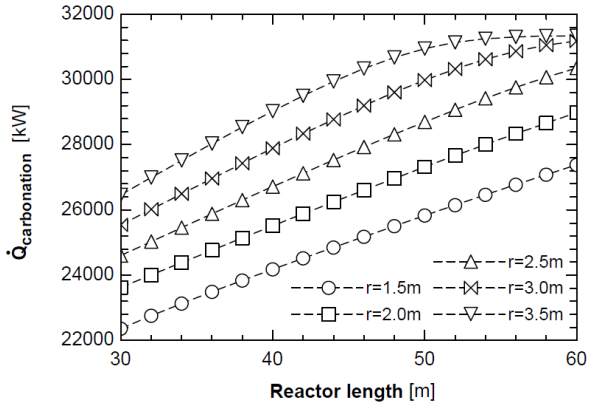

Figure 3. Total exothermal power vs reactor's length and radius dimensions.

The total heat removal by the cooling fluids (i.e., by the pressurized water for the Rankine cycle) is presented in Fig. 4. For those lengths described above that were set for 12% conversions, the thermal power removal is in the range 10.0 MW – 10.4 MW, which represents the 35.2% – 36.6% of the heat released during the reaction. In the case of a 7 m in diameter and 52 m in length reactor (13.2% conversion), the thermal power removal is about 14.0 MW, which accounts for the 45.0% of the exothermal energy from carbonation.

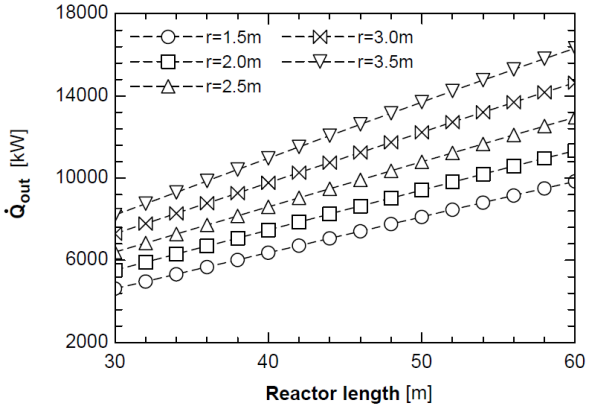

Figure 4. Total removed thermal power by cooling fluid vs. reactor's length and radius dimensions.

The remaining thermal power, which cannot be evacuated, heats the reactants and products inside the reactor up to the equilibrium temperature. As can be seen in Fig. 5, this situation takes place in the first meters of the carbonator. From here onwards, the conversion slowly increases as the heat is removed. In the depicted case in Fig. 5 (52 m in length and 7 m in diameter), the mass flows of cooling fluids c1, c2, c3 and c4 are 1.85 kg/s, 1.97 kg/s, 1.94 kg/s and 1.96 kg/s.

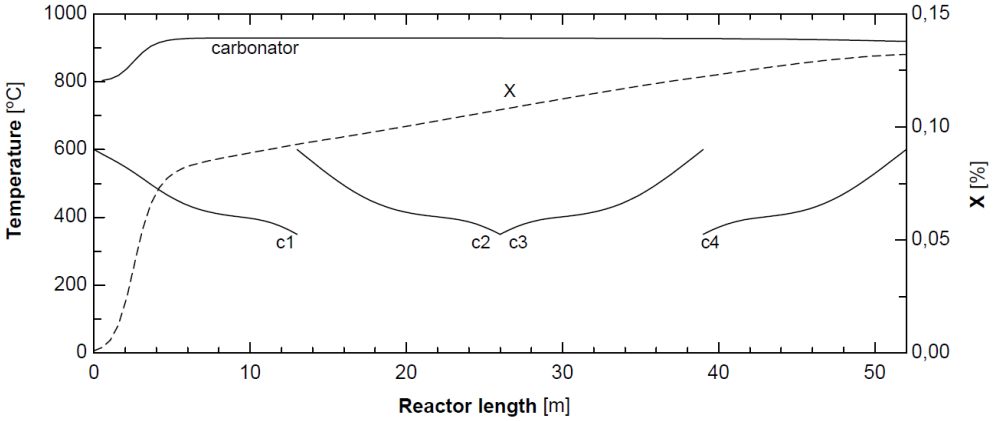

Figure 5. Temperatures and conversion profiles vs. axial position (L=52m, r=3.5m).

The carbonator's outlet gas-solid mixture can be cooled in order to recover more thermal power. In the case of the gas, it is separated from the solids, cooled down to 800 ºC, and recirculated to the carbonator's inlet. Thus, the available thermal power to be recovered from the gaseous CO_2 is presented in Fig. 6. It ranges from 8.0 MW to 8.2 MW for the 12% conversion configurations, thus accounting for about the 28% of the exothermal heat coming from the reaction. In the case of a reactor with 52 m in length and 7 m in diameter, this thermal power is 7.55 MW, what represents the 24% of the exothermal power.

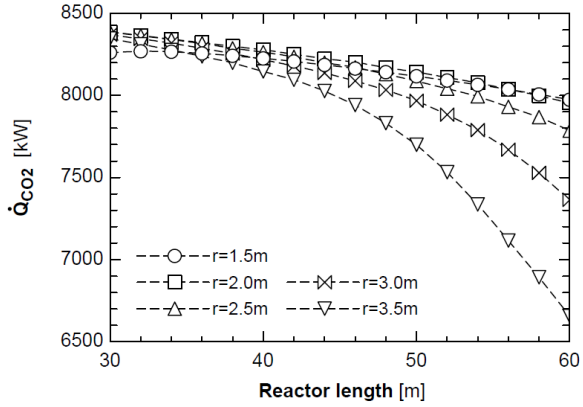

Figure 6. Available thermal power from CO_2 vs. reactor's length and radius dimensions.

The solids mixture is assumed to be cooled to 450 ºC, thus using this thermal power to heat more pressurized water. The available thermal power is presented in Fig. 7. In the case of 12% conversion configurations, it amounts between 37.7 MW and 38.3 MW. For the selected reactor of 52 m in length and 7 m in diameter, this available thermal power is 38.1 MW.

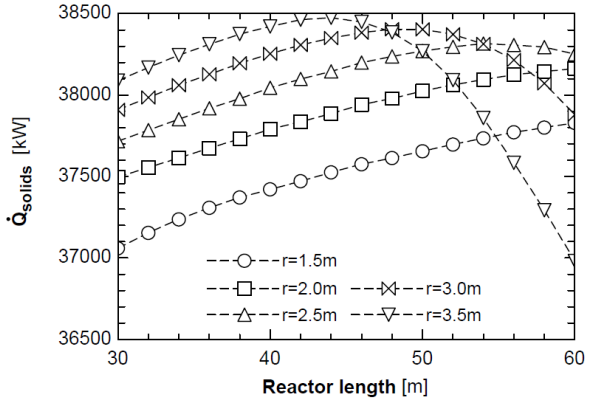

Figure 7. Available thermal power from solids vs. reactor's length and radius dimensions.

In total, if all the available thermal power is used, it amounts to 59.6 MW for the case of 13.2% conversion that is presented in Fig. 5. This represents the 59.6% of the total input solar power in the calciner. Thus, assuming a Ranking cycle efficiency of the 45%, the final round trip efficiency of the energy storage in terms of solar power to electricity production would be 26.8%.

5. Conclusions

In this work, the modelling of a future commercial-scale carbonator is described, in the frame of a new solar-based energy storage plant. The carbonator is a co-current entrained flow reactor covered with four helical coiled heat exchangers. The CaO and CO_2 inlet mass flow rates are 73.41 kg/s and 57.62 kg/s, respectively, which correspond to solar thermal powers of 100 MWth inside the calciner. Different lengths and diameters for the carbonator are analysed, as well as the corresponding heat released. The cooling fluid is pressurized water that enters the heat exchangers at 300 bar and 350 ºC and exits at 280 bar and 600 ºC.

The methodology takes geometry, heat transfer and calcination kinetics into account, thus obtaining the temperature profiles along the carbonator under non-isothermal conditions. The model is in steady-state, and the selected discretization divides the total length in 100 slices.

Results show that most of the exothermal heat from carbonation cannot be properly evacuated. Thus, most of the released thermal power rapidly heats the reactants and products inside the reactor up to the equilibrium temperature. This situation takes place in the first meters of the carbonator. From here onwards, the conversion slowly increases as the heat is removed. For a selected configuration of 52 m in length and 7 m in diameter, the final conversion is 13.2%, and the recovered thermal power from the four helical coiled heat exchangers amounts to 14 MW. The required mass flows of pressurized water are 1.85 kg/s, 1.97 kg/s, 1.94 kg/s and 1.96 kg/s. Moreover, if the carbonator's outlet gas-solid mixture is cooled down, it can be recovered 7.5 MW from the gaseous CO_2 and 38.1 MW from the solids mixture. Thus, the total thermal power finally used for the production of hot water is 59.6 MW, what represents a 59.6% of the inlet net solar power in the calciner.

Acknowledgments

The research leading to these results has received funding from the European Union's Horizon 2020 research and innovation programme under grant agreement No 727348, project SOCRATCES.

Nomenclature

Variables:

a_2	pre-exponential factor, 1/s
a	fitting parameter for the equilibrium pressure, K
A	specific projection area of the dispersed particles, m^2/kg
A_v	geometry-dependent absorptance of the gas body, -
$\mathcal{A}$	pre-exponential factor, atm
b	calculation parameter, 1/s
Cp	specific heat, kJ/(kmol·K)
d	diameter, m
E_2	carbonation activation energy, kJ/mol
f_p	pressure correction factor, -
g	gravity, m/s^2
Gz	Graetz number, -
h	convective heat transfer coefficient, $kW/(m^2 \cdot K)$
k	thermal conductivity, kW/(m·K)
K	emission or absorption coefficient of the gas phase, 1/m
l_{mb}	mean beam length, m
L	length, m
L_p	particle load at operation conditions, kg/m^3
$\dot{m}$	mass flow rate, kg/s
$\dot{n}$	mole flow rate, kmol/s
Nu	Nusselt number, -
P	pressure, bar
Pr	Prandtl number, -
$\dot{q}'$	heat flow per unit of length, kW/m
$\bar{Q}$	mean relative absorption or backscattering efficiency of a particle, -
r	reaction rate, 1/s
r	radius, m
R	thermal resistance, K/kW
Re	Reynolds number, -
$\mathcal{R}$	ideal gas constant, kJ/(kmol·K)
S_{eff}	effective cross-sectional area of reactor, m^2
t	reacting time or residence time, s
t_0	time to reach half of residual conversion, s
T	temperature, K
v	velocity, m/s
V	volume, m^3
$\dot{V}$	volumetric flow rate, m^3/s
X	conversion, -
X_k	residual conversion, -
ΔS_2^0	carbonation entropy change, J/(mol·K)
ΔH_2^0	standard enthalpy change of carbonation, kJ/mol
ΔH_r	enthalpy of carbonation, kJ/kmol

Greek symbols

α	absorptivity, -
β	calculation parameter, -
γ	calculation parameter, -
ε	emissivity, -
μ	viscosity, kg/(m·s)
ρ	density, kg/m^3
σ	Stefan-Boltzmann constant, $kW/(m^2 \cdot K^4)$
Φ	optical thickness for the gas solid dispersion, -

Subscripts and superscripts

abs	absorption
bsc	backscattering
c	carbonator
cf	cooling fluid
$conv$	convection
emi	emission
eq	equilibrium
g	gas
i	initial value or discretization index for axial position
in	inner
iw	inner wall

j	component j	rad	radiation
L	covered length	s	solid
out	outer radius or diameter	t	terminal velocity
ow	outer wall	$tube$	carbonator's tube
p	particle	w	wall

References

[1] Kearney D, Kelly B, Herrmann U, Cable R, Pacheco J, Mahoney R, et al. Engineering aspects of a molten salt heat transfer fluid in a trough solar field. Energy 2004;29:861–70. doi:10.1016/S0360-5442(03)00191-9.

[2] Kuravi S, Trahan J, Goswami DY, Rahman MM, Stefanakos EK. Thermal energy storage technologies and systems for concentrating solar power plants 2013. doi:10.1016/j.pecs.2013.02.001.

[3] Kyaw K, Matsuda H HM. Applicability of carbonation/decarbonation reactions to high-temperature thermal energy storage and temperature upgrading. J Chem Eng Jpn 1996;29:119–25.

[4] Romeo LM, Abanades JC, Escosa JM, Paño J, Giménez A, Sánchez-Biezma A, et al. Oxyfuel carbonation/calcination cycle for low cost CO2 capture in existing power plants. Energy Convers Manag 2008;49. doi:10.1016/j.enconman.2008.03.022.

[5] Lisbona P, Martínez A, Lara Y, Romeo LM. Integration of carbonate CO2 capture cycle and coal-fired power plants. A comparative study for different sorbents. Energy and Fuels 2010;24:728–36. doi:10.1021/ef900740p.

[6] Perejón A, Romeo LM, Lara Y, Lisbona P, Martínez A, Valverde JM. The Calcium-Looping technology for CO<inf>2</inf> capture: On the important roles of energy integration and sorbent behavior. Appl Energy 2016;162. doi:10.1016/j.apenergy.2015.10.121.

[7] Chacartegui R, Alovisio A, Ortiz C, Valverde JM, Verda V, Becerra JA. Thermochemical energy storage of concentrated solar power by integration of the calcium looping process and a CO 2 power cycle. Appl Energy 2016;173:589–605. doi:10.1016/j.apenergy.2016.04.053.

[8] Ortiz C, Chacartegui R, Valverde JM, Alovisio A, Becerra JA. Power cycles integration in concentrated solar power plants with energy storage based on calcium looping. Energy Convers Manag 2017;149:815–29. doi:10.1016/j.enconman.2017.03.029.

[9] Romano MC. Modeling the carbonator of a Ca-looping process for CO2 capture from power plant flue gas. Chem Eng Sci 2012;69:257–69. doi:10.1016/J.CES.2011.10.041.

[10] Ortiz C, Chacartegui R, Valverde JM, Becerra JA, Perez-Maqueda LA. A new model of the carbonator reactor in the calcium looping technology for post-combustion CO2 capture. Fuel 2015;160:328–38. doi:10.1016/J.FUEL.2015.07.095.

[11] Ortiz C, Valverde JM, Chacartegui R, Perez-Maqueda LA. Carbonation of Limestone Derived CaO for Thermochemical Energy Storage: From Kinetics to Process Integration in Concentrating Solar Plants. ACS Sustain Chem Eng 2018;6:6404–17. doi:10.1021/acssuschemeng.8b00199.

[12] Wen CY, Chaung TZ. Entrainment Coal Gasification Modeling. Ind Eng Chem Process Des Dev 1979;18:684–95. doi:10.1021/i260072a020.

[13] Kabelac S, Vortmeyer D. VDI Heat Atlas Part K - Radiation. In: VDI, editor. VDI Heat Atlas. Second, Springer-Verlag Berlin Heidelberg; 2010.

[14] Nellis G, Klein S. Heat transfer. Cambridge University Press; 2008.